Predicting Slope Deformation with Machine Learning

Naomi Eastwood
School of Surveying and Built Environment
University of Southern Queensland
naomi.m.eastwood@gmail.com

ABSTRACT

Accurate early warning systems are critical for mitigating the impact of landslides. With the increasing use of low-cost Global Navigation Satellite System (GNSS) monitoring systems, large and continuous datasets are becoming more available, enabling the application of machine learning to predict slope deformation. This paper is based on the author's undergraduate Honours research project at the University of Southern Queensland (UniSQ), which was awarded the APAS UniSQ Student Project Prize 2025. It explores if machine learning could forecast slope movement at Froggies Beach in Coolangatta and be used as an early warning system. A nonlinear autoregressive neural network with exogenous inputs (NARX) was trained on the monitoring data, with rainfall as an external input. The model achieved a root mean square error (RMSE) of 0.0015 m and a correlation coefficient (R^2) of 0.998 during testing. However, it failed to accurately predict large movement events. This is likely due to limitations in both the model structure and the available dataset. It was determined that the model would not be an effective early warning system, given that the major movement events are the most crucial to predict.

KEYWORDS: *GNSS, slope deformation prediction, machine learning, NARX.*

1 INTRODUCTION

The devastation caused by landslides can be severe. Globally, they resulted in the death of over 55,000 individuals between 2004 and 2016 and are estimated to cause approximately A$30 billion of losses annually (Sim et al., 2022). To reduce this impact, early warning systems that are capable of accurately predicting slope movement and failure are essential (Giordan et al., 2019; Sim et al., 2022). As low-cost Global Navigation Satellite System (GNSS) monitoring systems become more widely used, the continuous deformation data they collect allows for the exploration of machine learning models as early warning systems.

Developing an early warning system begins with collecting environmental observations of the natural processes affecting slope deformation (Giordan et al., 2019). Factors such as soil type, temperature, rainfall, groundwater fluctuations, vegetation and seismic activity can have an impact. The magnitude of influence of each factor will vary between sites (e.g. Li et al., 2024; Rahimi et al., 2011). Detailed environmental data is crucial and can be collected from soil testing, meteorological stations and piezometers (Giordan et al., 2019).

Accurately measuring site movement is essential for predicting slope deformation. Traditional surveying techniques with total stations provide highly accurate results, although survey costs can be high (Afeni and Cawood, 2013). Low-cost GNSS methods have been shown to achieve suitable accuracies for slope deformation monitoring (e.g. Cina and Piras, 2015; Hamza et al.,

2023) and since have been applied worldwide (e.g. Dong et al., 2020). Integration with communication networks and cloud-based analytics enables the remote collection of continuous, near-real-time monitoring data (Wang, 2023). These developments have made GNSS monitoring more feasible for smaller-scale applications, while the large datasets produced support the use of machine learning to predict site movement.

Prediction models for slope deformation can be generally classified as either physics-based or data driven (Gong et al., 2024). Physics-based models predict movement by accurately understanding the site-specific conditions and the mechanisms driving deformation. While they have been shown to accurately predict movement, they require extensive and detailed site information. Alternatively, data driven models, including machine learning, identify patterns within large datasets of environmental and deformation measurements, which are then used to construct predictive models. This approach can be advantageous, as the drivers of deformation do not need to be fully understood. However, such models require very large, continuous datasets for both slope deformation and influential environmental factors. Additionally, machine learning models are not easily generalised across sites, hence significant testing is necessary to determine whether a model can accurately predict slope deformation.

Machine learning is a form of data driven modelling that has been explored for predicting slope movement, with various model types shown to do so successfully. Artificial neural networks have been widely applied (Dong et al., 2020). Neural networks with long short-term memory (LSTM) have been shown to outperform standard neural networks (Zhang et al., 2021), with performance further improved using particle swarm optimisation (Wang et al., 2024) or attention mechanisms (Wang et al., 2021). However, model performance is strongly influenced by the availability of data. Van Natijne et al. (2023) applied an LSTM to predicted movement at the Vögelsberg landslide, Austria, but were unsuccessful due to limited training data. Nonlinear autoregressive neural networks with exogenous inputs (NARX) have successfully predicted other time-series relationships, such as groundwater fluctuations (Guzman et al., 2017; Wunsch et al., 2021), although their ability to predict slope deformation has not yet been evaluated.

This paper investigates the potential of machine learning to predict slope deformation at Froggies Beach, Coolangatta. To achieve this, the relationship between rainfall and slope deformation was analysed to better understand the dataset and identify potential drivers of movement. A NARX model was then trained, tested and evaluated to assess its suitability for predicting slope deformation at this site.

2 METHOD

2.1 Study Site

Froggies Beach is a small, sheltered beach in Coolangatta, Queensland, just north of the New South Wales border (Figure 1). Signs of slope creep were observed in the hill directly behind Froggies Beach, indicated by cracking in the footpath along the top of the hill and damage to the boardwalk descending to the beach. To better understand this movement, a GNSS monitoring survey was initiated in March 2021.

Figure 1: Google Earth image of the study site, i.e. the hill behind Froggies Beach, with the monitoring system (including monitoring and reference stations) indicated.

2.2 Monitoring Survey

2.2.1 Kurloo GNSS Monitoring System

Froggies Beach was monitored using the Kurloo technology monitoring system (Kurloo, 2026). This low-cost GNSS method, combined with cloud-based analytics, provides near-real-time daily positioning data. The system operates as differential GNSS, recording observations for several hours before transmitting the data for post-processing. A relative baseline between the monitoring stations and the reference station is then calculated for Easting, Northing and ellipsoidal height. The system can achieve an accuracy of ±4 mm horizontally and ±6 mm vertically at the 95% confidence level.

2.2.2 Froggies Beach Monitoring Data

The monitoring survey used a reference station initially installed near the site in a stable area (Wang, 2023). On 6 December 2023, it was removed and replaced by the Fingal Head Continuously Operating Reference Station (FGHD CORS), located within 1 km of the site and thereby meeting the positional accuracy requirements (J. Wang, pers. comm.). Two monitoring stations were installed within the area of concern: Node A halfway down the slope and Node B at the toe of the slope (see Figure 1).

This study used data from 4 March 2021 to 22 October 2024. Of the 1,329 days in this period, 1,137 observations were recorded for Node A and 1,140 observations for Node B. To increase the usability of the data for machine learning, gaps of three days or less were estimated from the mean of the adjacent days. After these estimations, the dataset contained 1,189 observations for Node A and 1,167 observations for Node B.

2.3 Environmental Data

2.3.1 Rainfall Data

Slope deformation occurs through the interaction of various factors in the natural environment, hence meteorological data is necessary to understand this relationship. Rainfall can be an influential factor, as it may increase groundwater levels, pore water pressure and soil pressure, potentially triggering slope movement (Li et al., 2024). Unfortunately, no rainfall or groundwater data was collected at the Froggies Beach site. Instead, rainfall records were obtained from the Bureau of Meteorology (BOM).

Two weather stations are located approximately 4 km from the site, i.e. the Coolangatta Airport station (040717) and the Tweed Heads Golf Club station (058056), which are about 5 km apart (Figure 2). Daily rainfall data from these stations showed a strong correlation, with a Pearson correlation coefficient of 0.944. This high level of agreement supports the inference that precipitation at Froggies Beach would be similar. Sub-daily rainfall data was only available from the Coolangatta Airport station – as this level of detail was required, data from this station was used.

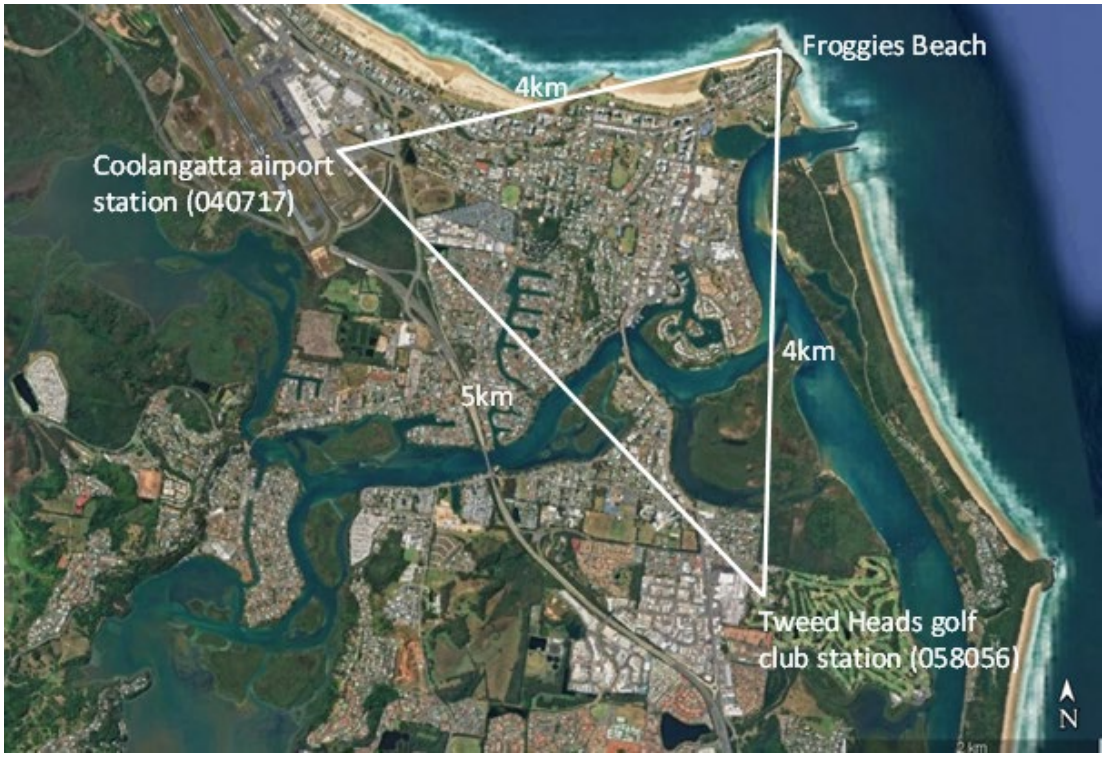

Figure 2: Google Earth image showing Froggies Beach and the BOM stations at Coolangatta Airport and the Tweed Heads golf club.

2.3.2 Soil Test

Soil type and its properties can strongly influence how a slope responds to external factors and whether movement occurs (Rahimi et al., 2011). A soil test completed on 8 May 2025 found the site to be high-plasticity sandy clay: 67% fines, 32% sand and 1% gravel (J. Wang, pers. comm.). The behaviour of the soil at this site was not further analysed in this study, as it was outside the scope of the research objectives.

2.4 Slope Deformation Analysis

The following calculations were applied to the monitoring data to calculate slope movement. The displacement in the aspect direction (d_{aspect}) was used in all further analysis as it represents movement in the likely failure direction. The difference in horizontal (Δx), vertical (Δy) and height (Δz) reference baselines, were calculated for daily displacement (the distance between consecutive daily positions) and cumulative displacement (the distance from the day one observation). The bearing (β) and slope (θ) of the hill were used to calculate the aspect vector ($\vec{a}$) in equation (1) and then normalised. The movement in the aspect direction (d_{aspect}) was subsequently calculated using equation (2) for both daily and cumulative displacement measurements.

$$\vec{a} = (\sin(\beta), \cos(\beta), \tan(\theta)) \quad (1)$$

$$d_{aspect} = \Delta x \cdot a_{norm,x} + \Delta y \cdot a_{norm,y} + \Delta z \cdot a_{norm,z} \quad (2)$$

2.5 Rainfall and Movement Analysis

The relationship between rainfall and slope deformation was explored to determine if there was a correlation and to justify the use of rainfall as a predictor in the machine learning model. Two analysis approaches were followed. Firstly, a comparison of daily movement and daily rainfall, and secondly, examining rainfall events and the associated movement response.

2.5.1 Daily Comparisons

Daily displacement was compared to daily rainfall by graphing the data to identify potential correlations. However, the relationship between rainfall and slope movement is often more complex than can be captured through day-to-day comparisons. The response time of a slope to rainfall can vary depending on the soil's infiltration rate (Li et al., 2024). To account for this, daily displacement was compared with rainfall data offset by 1-20 days. Additionally, antecedent rainfall (i.e. the rainfall occurring before a specific event such as a landslide) can be an important factor, as it indicates the saturation of the soil (Rahimi et al., 2011). Therefore, daily displacement was also compared to the cumulative rainfall over the previous 2-20 days, at 1-day intervals.

2.5.2 Event Comparisons

Analysing rainfall and displacement as discrete events allowed patterns to be identified in the characteristics of rainfall that preceded specific movement events, providing insight into the conditions that may trigger slope deformation. Gradual movement that occurred over several months was compared to monthly rainfall to explore whether prolonged deformation corresponded with particular rainfall levels.

The slope's more immediate response to rainfall was investigated by analysing discrete events. For each rainfall event, the following attributes were tabulated: the start and end date and time, total rainfall (mm), rate of rainfall (mm/hr), and the number of days since the previous rainfall event. Three-hourly rainfall data was used as it allowed a more precise calculation of the rate of rainfall.

The deformation data for the corresponding period was analysed to determine whether a response to rainfall occurred. Sandy clay soils, in which the clay particles dominate, have been

identified as highly reactive to groundwater fluctuations (Peters and Berney, 2010). Measuring both displacement and rebound allowed for the distinction between actual movement events and soil expansion. Where displacement was observed, the following information was recorded: the date when movement started and stopped, the total amount of downslope movement (mm), the total amount of rebound movement (mm) and the number of days the rebound occurred over. If no change in cumulative displacement was observed, this was noted.

The rainfall events were classified into the following groups:

- Resulted in significant movement (greater than 12 mm).
- Resulted in medium movement (between 8 mm and 12 mm).
- Resulted in no movement (less than 8 mm).

These categories were chosen based on the observation that the monitoring station typically did not fully rebound from movements greater than 12 mm. Since the accuracy of 3D displacement measurements was ±8 mm at the 95% confidence level, movements of less than 8 mm could not be confidently distinguished from measurement error and were treated as no movement. The values in these categories for rainfall quantity, rainfall rate and time since the previous event were then graphed, and the spread of values was examined. From this, consistent intervals for each variable were identified within the different movement groups.

2.6 Machine Learning

2.6.1 NARX Network

A nonlinear autoregressive network with exogenous inputs (NARX) model is a type of dynamic recurrent neural network (RNN) used for time series prediction, particularly for data with nonlinear relationships (Matlab Help Centre, 2026a). The model can generate predictions based solely on past outputs, but its performance can be improved by incorporating influential external variables as exogenous inputs (Leontaritis and Billings, 1985). While the NARX model is effective at capturing short-to-medium temporal dependencies, the model can struggle with long-term dependencies due to issues with vanishing and exploding gradients (Bengio et al., 1994). Nevertheless, the model is generally considered easy to implement and fast to train. In this study, the NARX model was selected to evaluate its ability to predict slope deformation.

The NARX model can be expressed by equation (3), where $y(t)$ represents the outputs and $u(t)$ the exogenous inputs at discrete time step t. The number of past values used by the model is defined by the time delay n. Each output is regressed on previous outputs and previous exogenous inputs. Structurally, the NARX model is a 2-layer feedforward network consisting of one hidden layer and one output layer (Figure 3). A sigmoid transfer function is applied within the hidden layer, enabling the network to assign weights to inputs and learn complex nonlinear relationships through gradient-based training. A linear transfer function is applied to the output layer, producing real-value predictions. Tapped time delay lines store the previous values of $y(t)$ and $u(t)$ sequences, which are then fed back into the network input (Matlab Help Centre, 2026c).

$$y(t) = f(y(t-1), y(t-2), \dots, y(t-n_y), u(t-1), u(t-2), \dots, u(t-n_u)) \qquad (3)$$

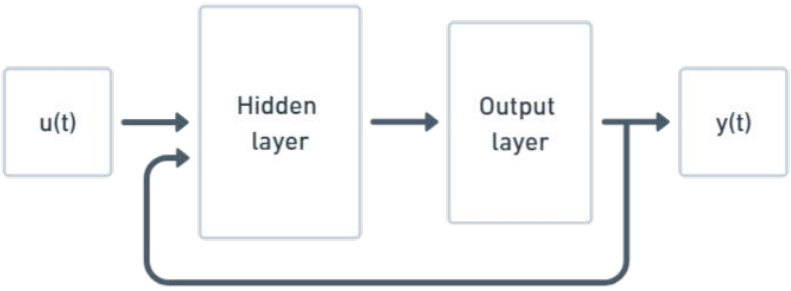

Figure 3: Flowchart of the NARX neural network structure with feedforward structure and feedback loop.

2.6.2 Input Parameters

The input parameters for the model included the continuous displacement data as the output value $y(t)$ and daily rainfall as an exogenous input $u(t)$.

2.6.3 Levenberg-Marquardt Training

The dataset was split into training, validation and testing data groups, with 55% used for training, 15% used for validation and 30% used for testing. The Levenberg-Marquardt function was used to train the model. This is a quasi-Newton method, which achieves faster training speeds by approximating the Hessian matrix (Matlab Help Centre, 2026d). The Levenberg-Marquardt algorithm can be defined as:

$$x_{k+1} = x_k - [J^T J + \mu I]^{-1} J^T e \tag{4}$$

The Jacobian matrix J contains the first derivatives of the errors with respect to the weights and biases, computed through a standard backpropagation technique. The network's errors are held in the vector e. The scaler μ defines the size of changes to the model parameters. When μ is large, gradient decent uses small step sizes, and once μ becomes smaller, the Newton's method is used to make larger confident steps, thus being faster and more accurate. A hold-out validation method was used where the performance metrics, root mean square error and coefficient of determination were calculated after each epoch (Matlab Help Centre, 2026d). This was used to evaluate model hyperparameters and stop training early.

2.6.4 Model Optimisation

The number of neurons in the hidden layer and the time delay were adjustable hyperparameters in the NARX model. A grid search was completed, testing all combinations of hidden layer sizes and time delays ranging from 1 to 5. Model performance was evaluated using the root mean square error (RMSE) and coefficient of determination (R^2) of the validation dataset. To account for variability due to random initialisations and to reduce the impact of outlier performance, an average of five results was taken. This process identified the optimal configuration as a hidden layer size of 3 and a time delay of 2. To further examine the effect of time delay, additional tests were conducted at intervals of 5 days up to 40 days while keeping the hidden layer size fixed at 3.

2.6.5 Model Evaluation

A model with a hidden layer size of 3 and a time delay of 2 was then evaluated on unseen test data. Model accuracy was determined by comparing predictions against actual values using two metrics. The RMSE, given in equation (5), expresses the average magnitude of prediction error, while the unadjusted coefficient of determination (R^2), given in equation (6), compares the trained model predictions to the constant mean of the training response (Matlab Help Centre, 2026b). Where y_i is the actual output value for observation i, $\hat{y}_i$ is the predicted value of output value for observation i, $\bar{y}$ is the mean of output values and n is the number of observations.

$$RMSE = \sqrt{\sum_{i=1}^{n} \frac{(\hat{y}_i - y_i)^2}{n}} \quad (5)$$

$$R^2 = \frac{\sum_i (\hat{y}_i - \bar{y})^2}{\sum_i (y_i - \bar{y})^2} \quad (6)$$

Response and error plots were used to visualise model performance and to determine how well the model captured slope behaviour during times of significant movement. Error autocorrelation plots were used to identify correlations in the residuals over time. In a perfect prediction model, the plot would show a single nonzero value at zero lag, with all other values behaving as uncorrelated white noise within the 95% confidence limits around zero (Matlab Help Centre, 2026c). In addition, input-error correlation graphs were used to determine whether past inputs were correlated with prediction errors. A perfect prediction model would display input-error correlations of zero.

3 RESULTS AND DISCUSSION

This study identified that there was a correlation between rainfall and slope deformation at Froggies Beach, justifying the use of rainfall as a predictor in the machine learning model. The performance of the NARX model as an early warning system was then evaluated. While the model demonstrated some capacity to estimate gradual movement, it failed to predict sudden and significant movement, reducing its effectiveness as a reliable early warning tool. The following discussion explores how, despite identifiable patterns in rainfall events preceding major deformation events, the structural constraints of the NARX model prevented it from remembering and applying these patterns. The impact of the limitations in the available dataset on model performance is also considered.

3.1 Slope Deformation

Over the data collection period, significant slope deformation was observed in the Froggies Beach hill, with Node A and Node B moving a total of 152 mm and 167 mm, respectively. The cumulative movement and rainfall are graphed in Figure 4. There were five times of significant movement, identified in red, and two periods of sustained gradual movement, identified in dark blue.

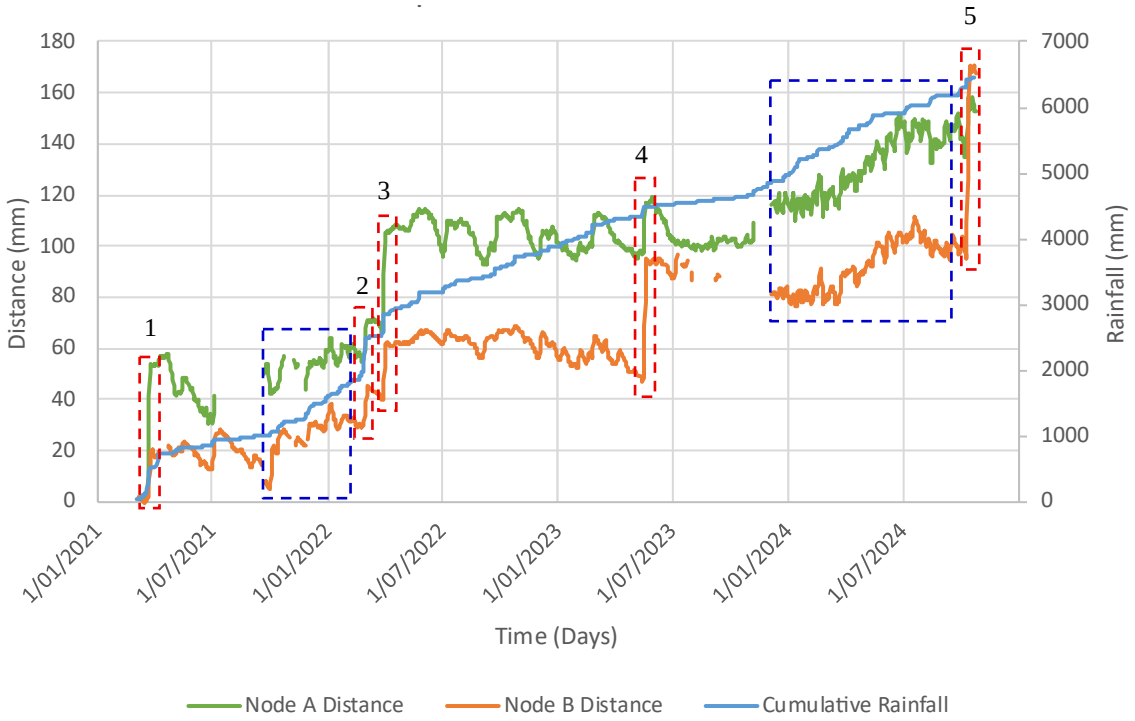

Figure 4: Cumulative displacement of the two monitoring stations, with cumulative rainfall shown in blue. Gradual movement events are identified in dashed dark blue and large movement events in dashed red.

3.2 Day-to-Day Analysis

Daily slope deformation showed a general correlation with daily rainfall (Figure 5), where increases in daily rainfall were often associated with increased daily movement. However, the relationship was non-linear, with several exceptions. These may be explained by a delayed slope response to rainfall. Cross-correlation analysis indicated that this relationship persisted for time lays of up to 5 days. Although this analysis confirmed the presence of a correlation, the daily temporal resolution was insufficient to provide detailed insights into the underlying processes.

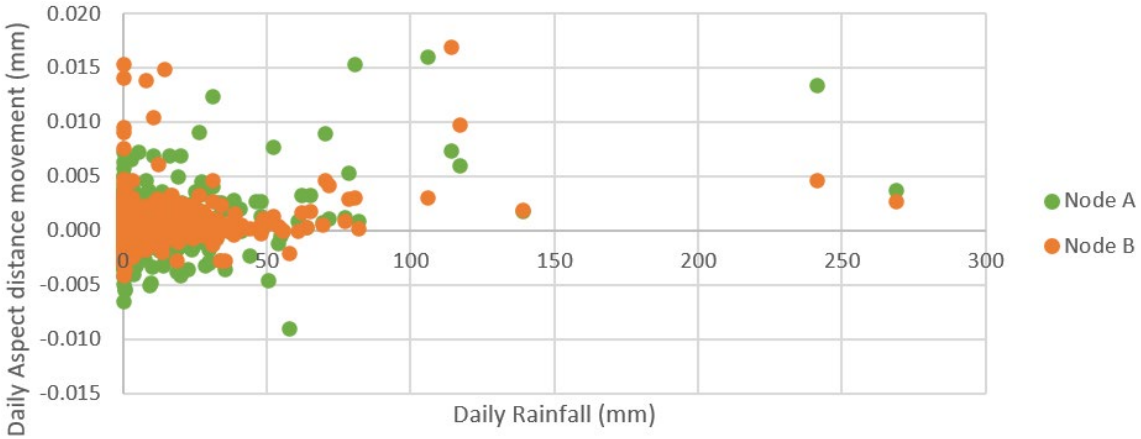

Figure 5: Correlation of daily rainfall and daily slope deformation, for each of the two monitoring stations.

3.3 Event Comparison

To better characterise the rainfall-movement relationship, the analysis shifted to an event-based approach. First, periods of sustained movement were examined alongside associated rainfall.

Second, short-term medium and large movement events were analysed, considering rebound and rainfall characteristics, allowing criteria for rainfall events preceding specific movement events to be identified.

3.3.1 Constant Movement

Two periods of sustained gradual movement were identified, indicated by the dashed dark blue boxes in Figure 4, occurring from December 2021 to February 2022 and from December 2023 until October 2024. During these intervals, incremental movements accumulated to approximately 20 mm. Figure 6 shows the total monthly rainfall over the monitoring period, with particularly high rainfall between December 2021 and March 2022. In contrast, rainfall in 2024 was more evenly distributed and greater in total volume, with 1,512 mm recorded between January and October, compared to 1,069 mm recorded across the entirety of 2023.

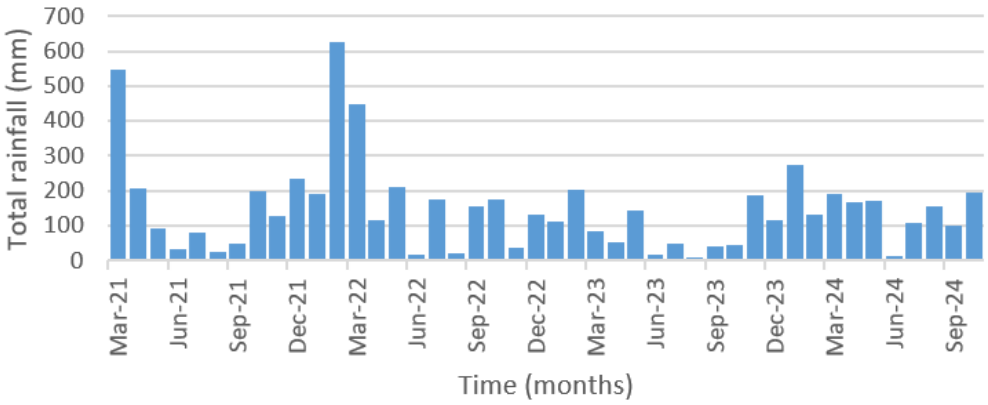

Figure 6: Total monthly rainfall for the data collection period recorded at the Coolangatta Airport BOM station (040717). Higher rainfall is evident from December 2021 to March 2022 and throughout 2024.

These observations indicate that periods of gradual movement are associated with sustained and relatively steady rainfall. Prolonged rainfall can result in a sustained increase in groundwater levels, leading to increased pore water pressure which, in combination with gravity, may accelerate slope movement (Ma et al., 2023). While this could explain the gradual movements observed, further analysis of soil and groundwater conditions would be required to confirm.

3.3.2 Rebounding of Movement Events

A key difference between medium and large movement events was the amount of rebound. Medium movements generally exhibited full rebound, whereas significant movement events did not. Figure 7 shows that movement events under 15 mm displayed a strong linear relationship between initial displacement and rebound, while larger movements showed no clear pattern. The site soil, identified to be sandy clay (with clay making up the majority), generally exhibits high compressibility and contraction during loading (Peters and Berney, 2010). The observed deformation likely reflects clay swelling followed by rebound as water drains or evaporates. However, detailed soil-groundwater analysis would be required to confirm this. Unlike medium events, large movements did not fully return to pre-event positions, indicating permanent displacement. These observations show that the type and magnitude of movement are affected by rainfall characteristics, which are examined in terms of quantity and rate in the following sections.

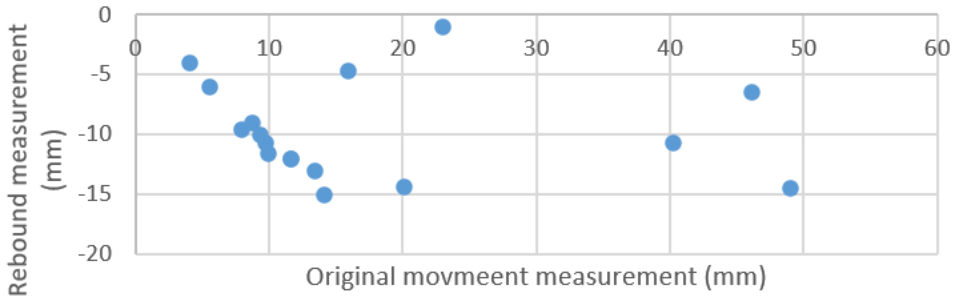

Figure 7: Original movement distances versus rebound quantity after the original movement, showing a linear correlation between the magnitude of the initial movement and rebound until the movement exceeds 15 mm.

3.3.3 Quantity of Rainfall

Rainfall quantity had a strong influence on the amount of movement observed (Figure 8), with large movement events generally following rainfall totals exceeding 120 mm, medium events occurring after 50-120 mm, and rainfall below 50 mm was typically associated with no movement. There were exceptions to these rules which are sometimes explained by the rate of rainfall (see section 3.3.4). In addition, the relationship was not linear. For example, movement event 2 occurred after the highest recorded rainfall event (580 mm) but resulted in only 13 mm of movement, whereas event 5 produced the greatest movement (75 mm at Node B) despite a comparatively modest rainfall quantity of 120 mm. While rainfall quantity affects increases in pore water pressure, the magnitude of this increase depends on other factors (Li et al., 2024). A more comprehensive understanding of the relationship between rainfall quantity and slope deformation requires analysis of groundwater infiltration and soil response.

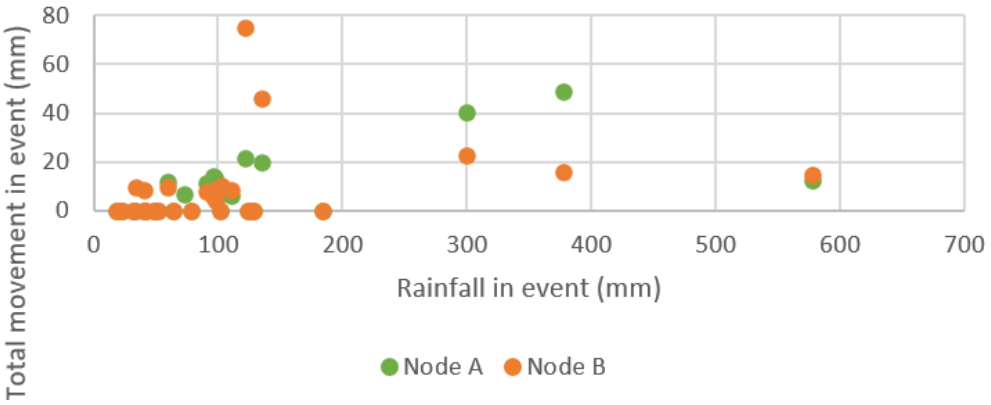

Figure 8: Quantity of rainfall in an event and the corresponding movement quantity for both monitoring stations.

3.3.4 Rate of Rainfall

The rate of rainfall during each event was compared with the total movement observed (Figure 9). Larger movement events generally occurred when rainfall rates were between 3 and 5 mm/hr, while medium-sized events were associated with rates of 1-3 mm/hr. No movement was observed when rainfall rates were below 1 mm/hr or exceeded 5 mm/hr. Observations at other sites suggest that high-intensity rainfall may promote surface runoff rather than infiltration, reducing subsurface changes that could trigger movement (Li et al., 2024). As with rainfall quantity, these thresholds represent general trends with exceptions, and site-specific analysis of soil and groundwater conditions would be required to fully explain the observed behaviour at Froggies Beach.

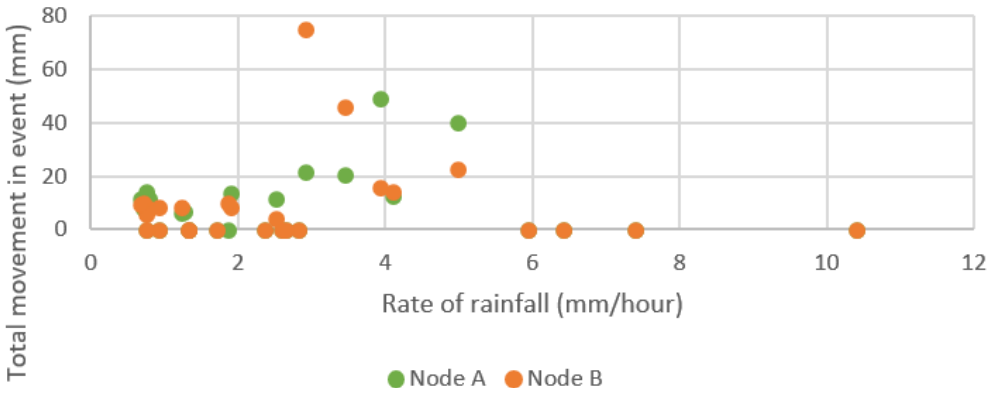

Figure 9: Rate of rainfall for the rainfall event versus the corresponding movement quantity for both monitoring stations.

3.3.5 Quantity of Rainfall and Rate of Rainfall Combined

The combination of rainfall quantity and rate was critical in determining the type of movement event. Figure 10 shows the rate and quantity of rainfall for each of the movement events, grouped by classification, revealing consistent rainfall characteristics preceding specific movement events. However, anomalies were observed, with some rainfall events exhibiting these characteristics without triggering movement. The timing between rainfall events was also considered, but there were not enough events in quick succession to establish clear patterns. Despite these limitations, the analysis confirmed a clear correlation between rainfall and movement, supporting the use of rainfall as a predictor in the machine learning model.

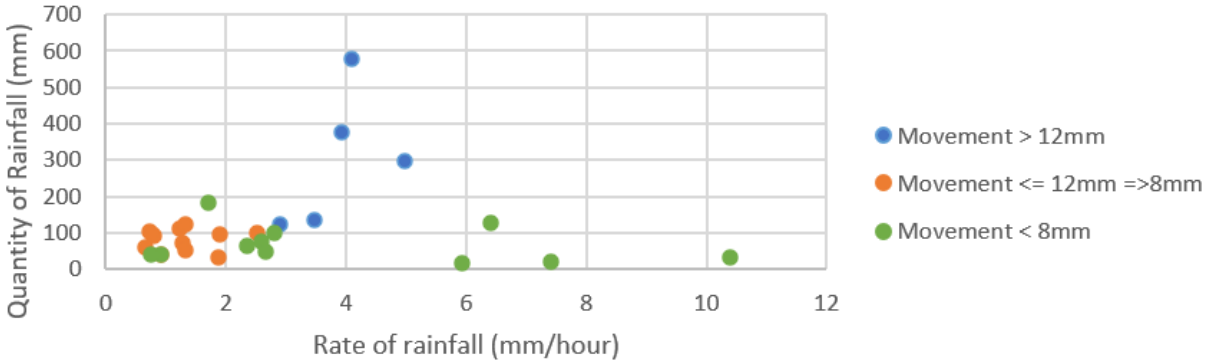

Figure 10: Rate of rainfall versus quantity of rainfall for the three classified movement groups (large, medium and no movement).

3.3.6 Limitations of Rainfall and Slope Deformation Correlation

The analysis revealed a correlation between rainfall and slope deformation, with some consistent characteristics of rainfall events preceding specific movements. However, the level of understanding of the relationship was limited by environmental data constraints. Site-specific rainfall measurements and groundwater monitoring would provide more accurate and meaningful insights, as groundwater may be a primary driver of slope deformation. The available temporal resolution also limited analysis; sub-daily monitoring could clarify the timing of movement relative to rainfall. The accuracy of measurements would have to be considered, as increases in noisy data may not necessarily enhance understanding. Despite these limitations, the observed relationship supports the use of rainfall as a predictor in the machine learning model.

3.4 Machine Learning

Machine learning provides a method of predicting slope deformation, without requiring a complete understanding of the underlying movement processes, and its ability to utilise large datasets makes it well suited to the Froggies Beach site. Combinations of hyperparameters were tested to identify the optimal configuration, followed by evaluation of model performance, which revealed limitations in the models' ability to accurately predict movement.

3.4.1 Model Optimisation

The evaluation of model hyperparameters showed that the best-performing model had a hidden layer size of 3 and a time delay of 2. From the grid search, Figure 11 shows the validation RMSE and R^2.

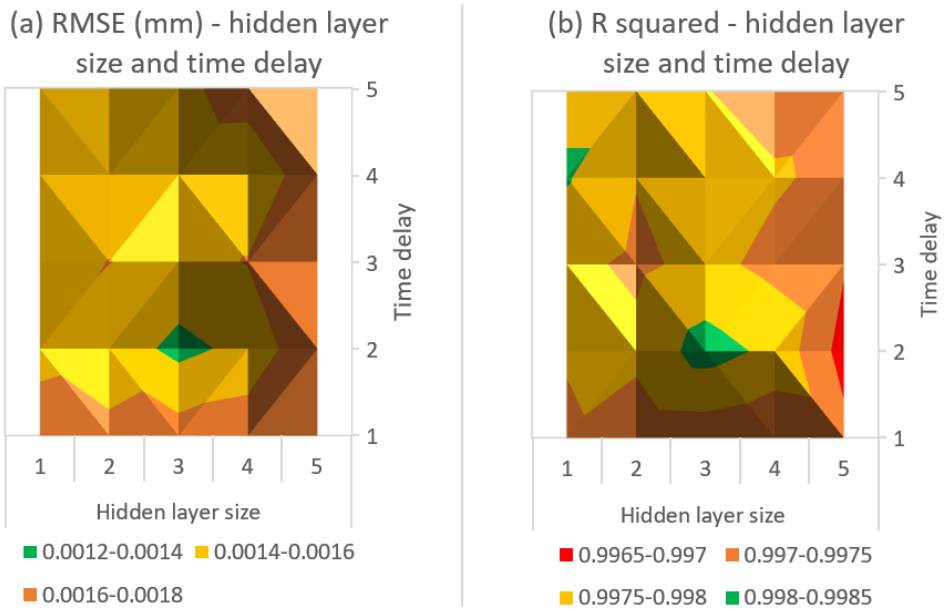

Figure 11: Grid search results for combinations of hyperparameters (hidden layer size versus time delay) for (a) the validation RMSE (closest to 0 is green and furthest from 0 is orange), and (b) the validation R^2 (closest to 1 is green and furthest from 1 is red).

Figure 11 indicates that model performance declined when the hidden layer size exceeded 4, while performance improved with time delays greater than 1. However, as shown in Figure 12, comparison of the training and testing R^2 values revealed that increasing the time delay beyond 10 days led to overfitting.

Figure 12: Comparison of the training R^2 value (blue) and the testing R^2 value (orange) for increasing time delays.

3.4.2 NARX Model Performance

The performance of the final NARX model indicated that it could accurately predict slope deformation (Table 1). The model achieved an RMSE of 0.0015 m, which is within the accuracy limits of the monitoring equipment, and an R^2 of 0.998. However, the following graphs, which further explore model behaviour, suggest there are underlying issues.

Table 1: The RMSE and R^2 values of the NARX model on displacement data from Node A and Node B.

Deformation Dataset	RMSE (m)	R^2
Node A	0.0015	0.998
Node B	0.0012	0.998

Figures 13 & 14 visualise the output of the NARX model, with training outputs in blue, validation outputs in green, and test outputs in red. The model errors are shown in orange. For most of the time period, the error in the model was within ±0.005 m, which is reasonable given the monitoring equipment has an accuracy of ±0.008 m. However, this error noticeably increases during times of large movement, reaching up to +0.015 m. The error also increases during times of gradual movement, particularly at the end of the time period at Node A (see Figure 14). This undermines the model's ability as an early warning system, as large movement is the most essential to accurately predict.

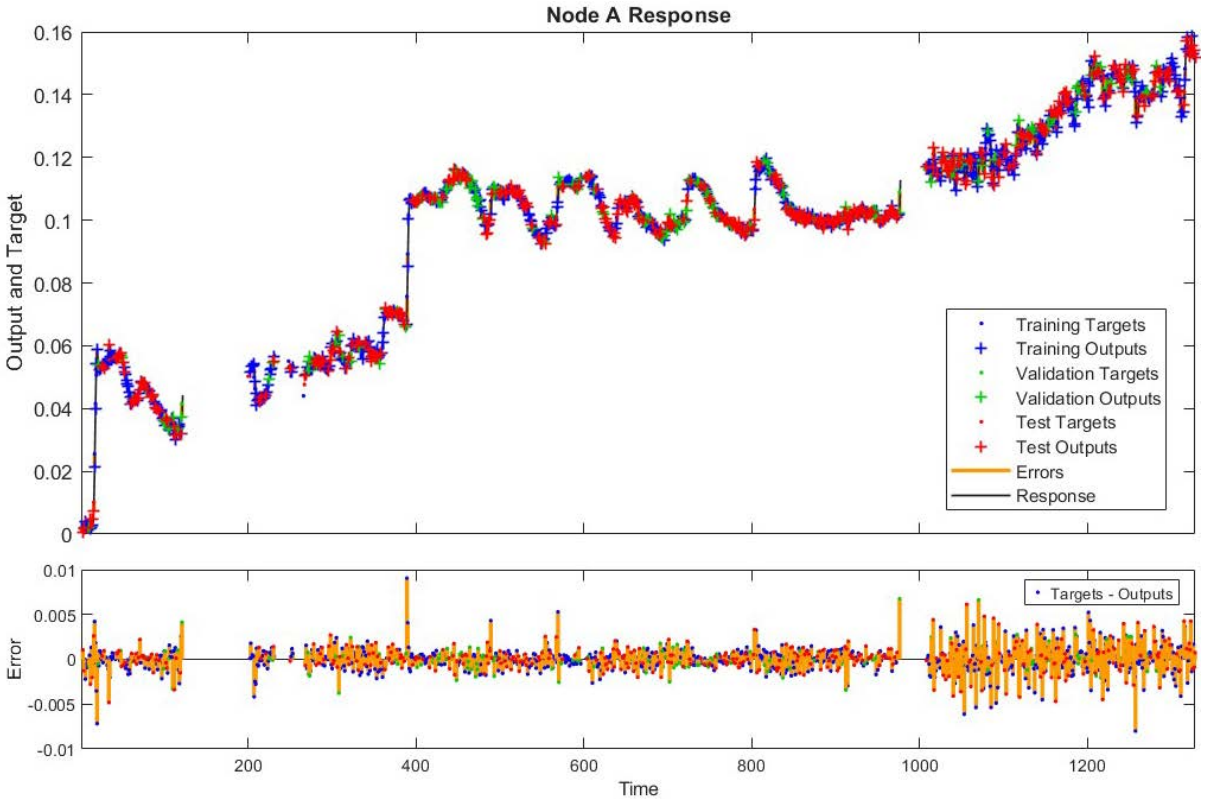

Figure 13: Node A response, showing the training outputs (blue), validation outputs (green) and test outputs (red), with cumulative slope displacement (in metres) versus time. The error between the model prediction and actual value is shown in the error plot in orange.

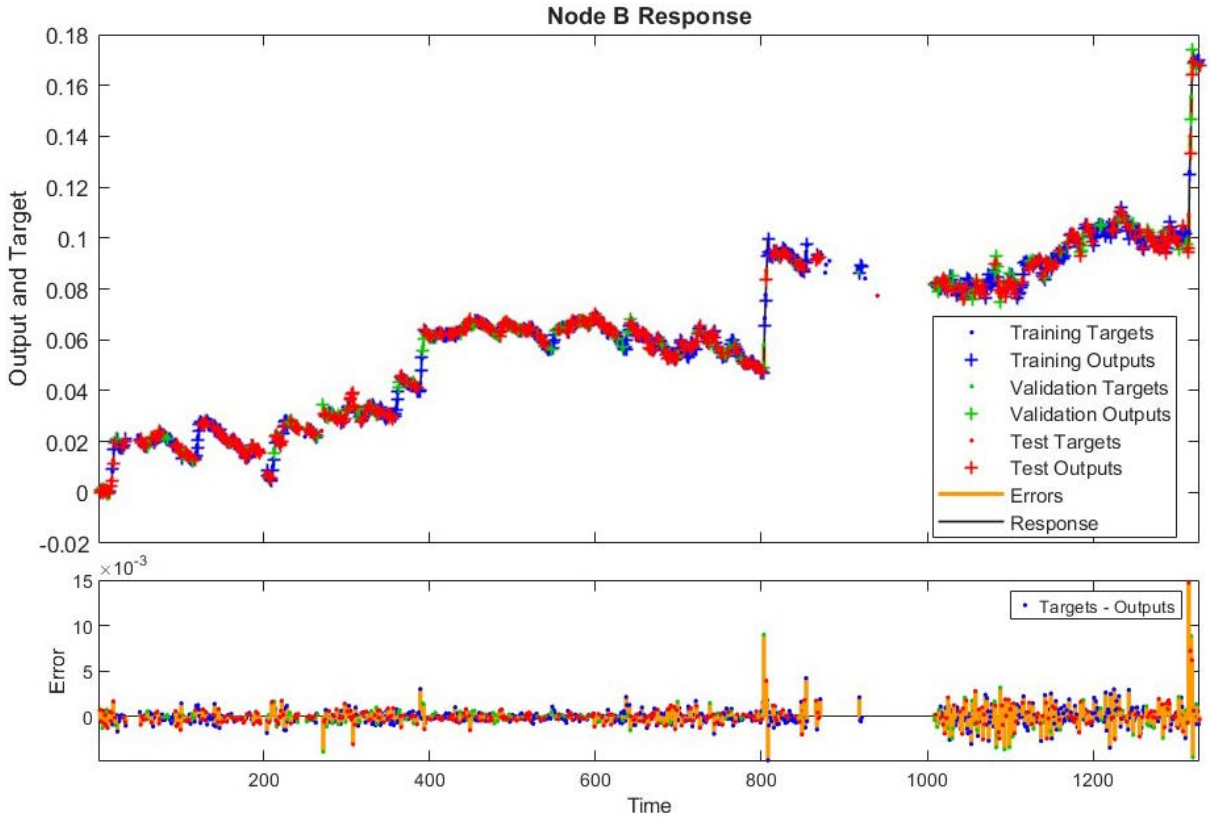

Figure 14: Node B response, showing the training outputs (blue), validation outputs (green) and test outputs (red), with cumulative slope displacement (in metres) versus time. The error between the model prediction and actual value is shown in the error plot in orange.

3.4.3 Failure to Learn Input-Output Dynamics

The autocorrelation graphs (Figure 15) show a high correlation between the errors at time step ±3 for Node A and ±5 for Node B, indicating the current errors are influenced by errors occurring several steps earlier or later. This pattern suggests oscillating error behaviour, where the model systematically over- or underestimates displacement at regular intervals rather than producing randomly distributed errors.

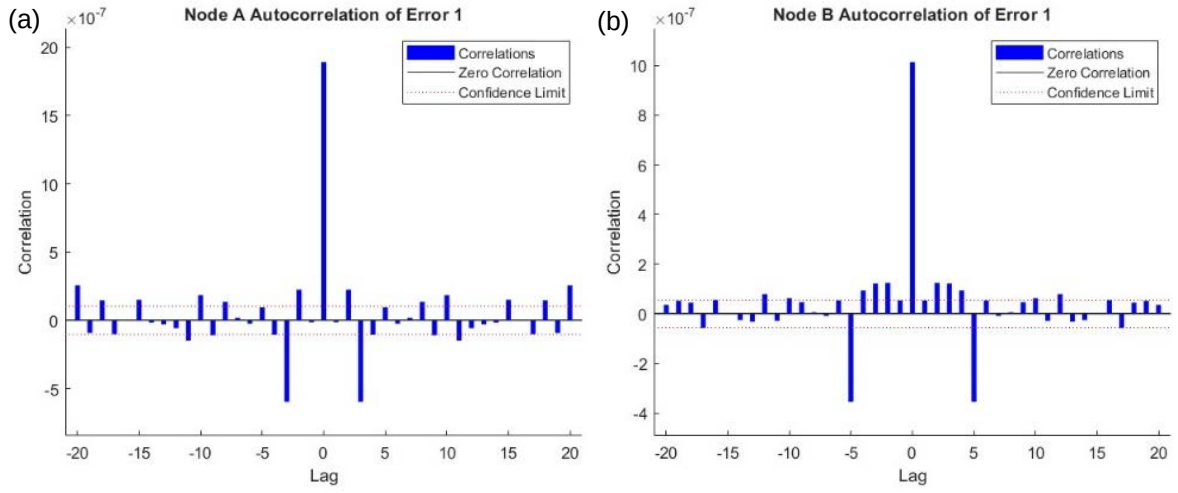

Figure 15: Autocorrelation of the NARX model for (a) Node A and (b) Node B. A perfect model would only have a correlation at lag 0, the high correlation at approximately lag 5 at both nodes suggests problems in the model's performance.

The input-error correlation graph (Figure 16) shows high correlation between prediction errors and the rainfall input, indicating that the model does not fully capture the effect of rainfall on slope displacement. Together, these observations indicate suboptimal model performance, suggesting the NARX model has failed to learn the relationship between rainfall and slope deformation and is instead relying on autoregressive patterns in the output data.

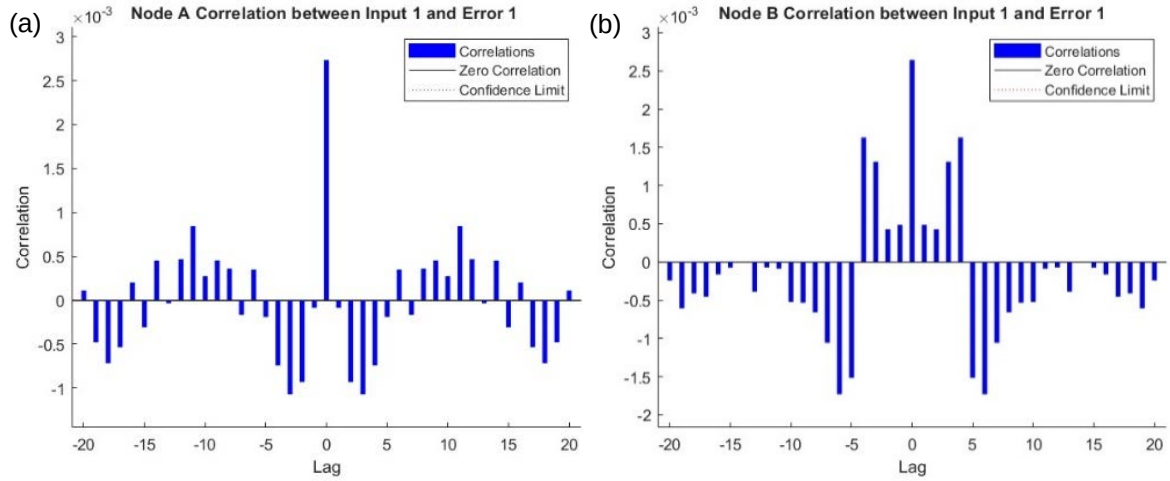

Figure 16: Input-error correlation of the NARX model for (a) Node A and (b) Node B. A perfect model would have correlations close to zero, i.e. the higher correlations and patterns in the graph suggest problems with model performance.

The NARX model is designed to regress the current output (slope movement) on past outputs and exogenous inputs (rainfall). By learning the dynamic relationship between inputs and outputs, the model should improve its prediction of slope deformation (Matlab Help Centre, 2026a). However, in this case the model failed to capture the influence of rainfall on slope movement. Instead, it became overly dependent on autoregressive feedback, relying primarily on past slope movement rather than responding to rainfall inputs. As a result, the model struggled to predict changes in movement associated with rainfall events.

Data that more accurately captures the relationships between environmental factors and slope deformation may lead to more effective predictions. Incorporating groundwater measurements alongside rainfall would provide a more complete representation of the drivers of movement, potentially improving predictions (Dong et al., 2020; Wang et al., 2021). Increasing the frequency of monitoring data to sub-daily intervals would allow the use of sub-daily rainfall data, offering a more precise representation of both the rate of movement and rate of rainfall. However, the noise in the data would have to be considered, as noisy data would more likely degrade the model performance rather than improve it.

3.4.4 Model Structure Limitations

The model's predictions for significant movement events were poor, largely due to the memory limitations of the NARX model. Model memory is determined by the selected time delay, as information outside this window is not retained. Consequently, the model is trained only on patterns observed within the defined time delay period (Menezes Jr and Barreto, 2008). As the large movement events all fell outside the 2-day time delay, the model was unable to learn these patterns or reproduce them in its predictions. Increasing the time delay was not a solution as the model became overfitted. Alternative model structures may overcome these limitations and improve predictive performance.

Other machine learning approaches may better capture the temporal dependencies in this dataset. LSTM models use memory cells to retain long-term information, improving predictions for rate events (Goodfellow et al., 2016), while attention mechanisms (AMs) can further emphasise such events and improve the model's understanding of the correlation (Wang et al., 2021). However, data availability remains a critical limitation. Van Natijne et al. (2023) found that an LSTM trained on three years of daily data was unable to accurately predict creep slope deformation. They concluded that the small dataset meant the model encountered some situations only a few times, or not at all, resulting in inaccurate predictions. Therefore, even with a more appropriate model structure, the limited data at Froggies Beach and the infrequent occurrence of significant movement may continue to hinder accurate slope deformation predictions.

4 CONCLUDING REMARKS

This paper has evaluated the use of a NARX model to predict slope deformation at Froggies Beach with rainfall as an external input. While analysis identified patterns in the rainfall events and subsequent slope movement, the model was unable to learn the underlying input-output dynamics. This is likely due to limitations in both the model architecture and the available dataset. It was found that the NARX model would not be appropriate as an early warning system for Froggies Beach. Future research could investigate if alternative model structures, such as AM-LSTM networks, could overcome these issues.

ACKNOWLEDGEMENTS

This paper is based on the author's undergraduate Honours research project at the University of Southern Queensland (UniSQ), which was awarded the APAS UniSQ Student Project Prize 2025. The Kurloo team, particularly Lee Hallen and Jun Wang, are gratefully acknowledged for generously sharing the dataset, without which this study would not have been possible. Prof Kevin McDougall and Dr Bikram Banerjee are thanked for their continual help. Finally, thank you to DSQ Land Surveyors, my friends and my family for their support and encouragement throughout this project.

REFERENCES

Afeni T.B. and Cawood F.T. (2013) Slope monitoring using total station: What are the challenges and how should these be mitigated? *South African Journal of Geomatics*, 2(1), 41-53.

Bengio Y., Simard P. and Frasconi P. (1994) Learning long-term dependencies with gradient descent is difficult, *IEEE Transactions on Neural Networks*, 5(2), 157-166.

Cina A. and Piras M. (2015) Performance of low-cost GNSS receiver for landslides monitoring: Test and results, *Geomatics, Natural Hazards and Risk*, 6(5-7), 497-514.

Dong M., Wu H., Hu H., Azzam R., Zhang L., Zheng Z. and Gong X. (2020) Deformation prediction of unstable slopes based on real-time monitoring and deepar model, *Sensors*, 21(1), 14.

Giordan D., Wrzesniak A. and Allasia P. (2019) The importance of a dedicated monitoring solution and communication strategy for an effective management of complex active landslides in urbanized areas, *Sustainability*, 11(4), 946.

Gong W., Zhang S., Juang C.H., Tang H. and Pudasaini S.P. (2024) Displacement prediction of landslides at slope-scale: Review of physics-based and data-driven approaches, *Earth-Science Reviews*, 258, 104948.

Goodfellow I., Bengio Y. and Courville A. (2016) *Deep learning*, MIT Press, Cambridge, Massachusetts, 800pp.

Guzman S.M., Paz J.O. and Tagert M.L.M. (2017) The use of NARX neural networks to forecast daily groundwater levels, *Water Resources Management*, 31(5), 1591-1603.

Hamza V., Stopar B., Sterle O. and Pavlovčič-Prešeren P. (2023) A cost-effective GNSS solution for continuous monitoring of landslides, *Remote Sensing*, 15(9), 2287.

Kurloo (2026) How our technology works, https://www.kurloo.io/kurloo-gnss/ (accessed Mar 2026).

Leontaritis I.J. and Billings S.A. (1985) Input-output parametric models for non-linear systems part I: Deterministic non-linear systems, *International Journal of Control*, 41(2), 303-328.

Li L., Li Y. and Xu Y. (2024) Instability evolution of expansive soil slope due to short duration-varying intensities of rainfall, *Engineering Failure Analysis*, 161, 108313.

Ma S., Qiu H., Zhu Y., Yang D., Tang B., Wang D., Wang L. and Cao M. (2023) Topographic changes, surface deformation and movement process before, during and after a rotational landslide, *Remote Sensing*, 15(3), 662.

Matlab Help Centre (2026a) Design time series NARX feedback neural networks, https://au.mathworks.com/help/deeplearning/ug/design-time-series-narx-feedback-neural-networks.html (accessed Mar 2026).

Matlab Help Centre (2026b) Root Mean Square Error (RMSE), https://au.mathworks.com/help/matlab/ref/rmse.html#mw_e6dea0e6-696e-4998-b5c2-369249b2987a (accessed Mar 2026).

Matlab Help Centre (2026c) Shallow neural network time-series prediction and modeling, https://au.mathworks.com/help/deeplearning/gs/neural-network-time-series-prediction-and-modeling.html (accessed Mar 2026).

Matlab Help Centre (2026d) Trainlm Levenberg-Marquardt backpropagation, https://au.mathworks.com/help/deeplearning/ref/trainlm.html (accessed Mar 2026).

Menezes Jr J.M.P. and Barreto G.A. (2008) Long-term time series prediction with the NARX network: An empirical evaluation, *Neurocomputing*, 71(16-18), 3335-3343.

Peters J.F. and Berney E.S. (2010) Percolation threshold of sand-clay binary mixtures, *Journal of Geotechnical and Geoenvironmental Engineering*, 136(2), 310-318.

Rahimi A., Rahardjo H. and Leong E.-C. (2011) Effect of antecedent rainfall patterns on rainfall-induced slope failure, *Journal of Geotechnical and Geoenvironmental Engineering*, 137(5), 483-491.

Sim K.B., Lee M.L. and Wong S.Y. (2022) A review of landslide acceptable risk and tolerable risk, *Geoenvironmental Disasters*, 9, 3.

van Natijne A.L., Bogaard T.A., Zieher T., Pfeiffer J. and Lindenbergh R.C. (2023) Machine-learning-based nowcasting of the Vögelsberg deep-seated landslide: Why predicting slow deformation is not so easy, *Natural Hazards and Earth System Sciences*, 23(12), 3723-3745.

Wang J. (2023) Kurloo: The GNSS-IoT solutions for continuous monitoring of embankment instabilities applied to Froggy Beach (Gold Coast, Queensland, Australia), *Proceedings of 14th Australia and New Zealand Conference on Geomechanics (ANZ2023)*, Cairns, Australia, 2-5 July, 5pp.

Wang J., Nie G., Gao S., Wu S., Li H. and Ren X. (2021) Landslide deformation prediction based on a GNSS time series analysis and recurrent neural network model, *Remote Sensing*, 13(6), 1055.

Wang S., Lyu T.-l., Luo N. and Chang P. (2024) Deformation prediction of rock cut slope based on long short-term memory neural network, *International Journal of Machine Learning and Cybernetics*, 15(3), 795-805.

Wunsch A., Liesch T. and Broda S. (2021) Groundwater level forecasting with artificial neural networks: A comparison of long short-term memory (LSTM), convolutional neural networks (CNNs), and non-linear autoregressive networks with exogenous input (NARX), *Hydrology and Earth System Sciences*, 25(3), 1671-1687.

Zhang X., Zhu C., He M., Dong M., Zhang G. and Zhang F. (2021) Failure mechanism and long short-term memory neural network model for landslide risk prediction, *Remote Sensing*, 14(1), 166.